Volume 1 | Number 1 | Jan 2013 | Pages 1–100

Nanoscale

www.rsc.org/nanoscale

ROYAL SOCIETY OF CHEMISTRY

ROYAL SOCIETY OF CHEMISTRY

www.rsc.org/nanoscale

Journal Name

Aqueous phase preparation of ultrasmall MoSe₂ nanodots for efficient photothermal therapy of cancer cells

Lihui Yuwen,[a] Jiajia Zhou,[a] Yuqian Zhang,[a] Qi Zhang,[a] Jingyang Shan,[a] Zhimin Luo,[a] Lixing Weng,[b] Zhaogang Teng,[c] and Lianhui Wang*[a]

Photothermal therapy (PTT) is a promising cancer treatment with both high effectiveness and less side effect. However, an ideal PTT agent not only needs strong absorption of near-infrared (NIR) light and high photothermal conversion efficiency, but also needs good biocompatibility, stability, and small size, which makes the design and preparation of novel PTT agent a great challenge. In this work, we developed an ultrasonication-assisted liquid exfoliation method for the direct preparation of ultrasmall MoSe₂ NDs (2-3 nm) in aqueous solution and demonstrate their superior properties as PTT agent. The as-prepared MoSe₂ NDs have strong absorption of NIR light and high photothermal conversion efficiency about 46.5%. In vitro cellular experiments demonstrate that MoSe₂ NDs have neglectable cytotoxicity and can efficiently kill HeLa cells (human cervical cell line) under NIR laser (785 nm) irradiation.

Introduction

PTT is an effective method to kill cancer cells by using local high temperature induced by PTT agents under laser irradiation.[1-2] Compared with conventionally used treatments of cancer, such as surgery, chemotherapy, radiation therapy, and so on, PTT has less invasive damage to lateral normal tissues and has been considered as a promising alternative for oncotherapy.[3-4] Benefited from the rapidly developing nanotechnology and biophotonics, PTT has gained great progress and attracted extensive attention from basic research to clinical medicine.[3, 5-7] During the past decay, plenty of materials have been explored as PTT agents, such as carbon nanomaterials, Au nanostructures, copper chalcogenides, organic dyes, and polymer nanoparticles.[8-14] For an ideal PTT agent, several features should be satisfied at the same time, including high extinction coefficient in NIR region (700-1400 nm), high photothermal conversion efficiency, low cytotoxicity, small size, and so on.[4, 15] Although many types of PTT agents have been studied, they usually have their own drawbacks. For example, organic dyes, like the FDA approved indocyanine green (ICG), have very small size and can be easily cleaned

from the body, but they are not stable and often tend to photobleach quickly under intense laser irradiation.[16-17] Inorganic nanomaterial PTT agents are usually photostable, but most of them have low heat generation efficiency and large sizes from tens to hundreds of nanometres which are too large for effective renal clearance from the body and will bring the low-term toxicity concern.[4, 18] In order to solve this problem, to develop novel PTT agents with ultrasmall size (<10 nm) have been realized as a feasible strategy, recently. Until now, very few ultrasmall PTT agents have been reported.[19-22] Moreover, to design or find novel materials, which can simultaneously satisfy all of the requirements needed by ideal PTT agent, is even more challenging.

During recent years, two-dimensional (2D) layered transition metal dichalcogenides (TMDCs) with generalized formula MX₂ (M, transition metal atoms; X, chalcogen atoms), including MoS₂, WS₂, TiS₂, etc., have drawn great attention.[23] After exfoliated to single-layer or few-layers, TMDCs nanosheets can exhibit novel electronic and optical properties compared with their bulk forms due to quantum confinement effect, which boosts many exciting applications.[24] In contrast to the extensively studied 2D TMDCs nanosheets, zero-dimensional (0-D) TMDCs NDs or QDs (quantum dots) with ultrasmall size haven't been well studied yet, although some recent reports have shown their potential applications for excellent catalysts, energy storage, biosensing, and bioimaging.[25-29]

Several techniques have been used to prepare TMDCs NDs, such as hydrothermal method and electrochemical synthesis,[25, 29-31] but their reliability, generality, and versatility are still not satisfactory, which hinders further study of TMDCs NDs.[28, 32] Recently, Zhang et al. developed a sonication-assisted liquid exfoliation method, which is a facile and reliable route to

a. Key Laboratory for Organic Electronics and Information Displays & Institute of Advanced Materials (IAM), Jiangsu National Synergetic Innovation Centre for Advanced Materials (SICAM), Nanjing University of Posts & Telecommunications, 9 Wenyuan Road, Nanjing 210023, China.
b. School of Geography and Biological Information, Nanjing University of Posts & Telecommunications, Nanjing 210023, China.
c. Department of Medical Imaging, Jinling Hospital, Clinical School of Medical College, Nanjing University, Nanjing 210002, China.
* Authors to whom correspondence should be addressed;
Tel.: +86 25 85866333; Fax: +86 25 85866396.
E-mail: iamlhwang@njupt.edu.cn

prepare TMDCs NDs.[33] Due to the use of organic solvents, such as N-methyl-2-pyrrolidone (NMP), to further explore the applications of TMDCs NDs in aqueous environment will need complicated surface functionalization and phase transfer process. Therefore, to develop direct preparation approach of TMDCs NDs in aqueous solution is still needed, especially for expanding their potential applications to biomedicine.
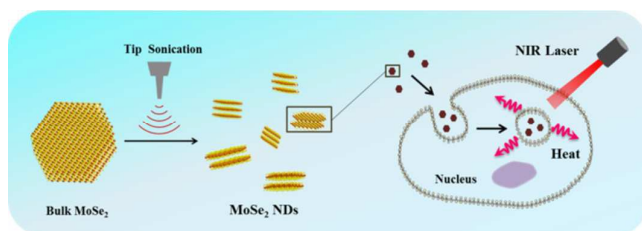
Scheme 1. Direct preparation of $MoSe_2$ NDs in aqueous solution by ultrasonication-assisted exfoliation and their use as novel photothermal agent to treat cancer cells.

In this report, we developed a facile and direct preparation method of ultrasmall $MoSe_2$ NDs in aqueous solution with the assistance of ultrasonication. More intriguingly, $MoSe_2$ NDs have significant NIR absorption and excellent photothermal conversion ability. Encouraged by the unique optical properties of $MoSe_2$ NDs, we investigate their photothermal stability, colloidal stability, cytotoxicity, and evaluate their potential use as a novel photothermal agent in vitro.

Results and discussion
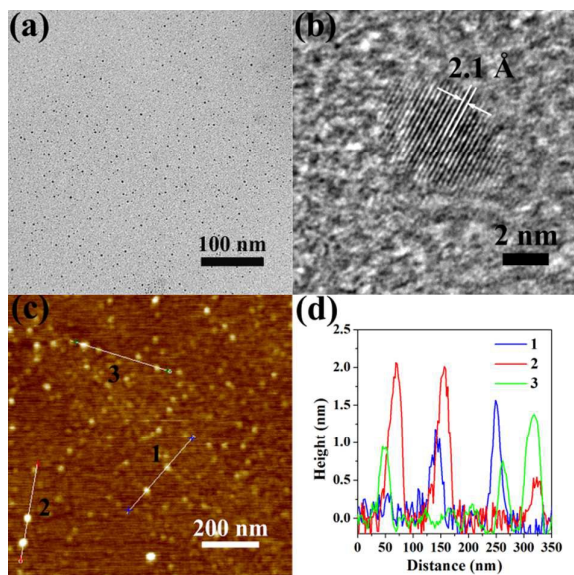
Fig. 1 (a) Transmission electron microscopy (TEM) images of $MoSe_2$ NDs; (b) High-resolution transmission electron microscopy (HRTEM) images of $MoSe_2$ NDs; (c) Atomic force microscopy (AFM) images and (d) height profiles of $MoSe_2$ NDs.

Preparation of $MoSe_2$ NDs

$MoSe_2$ NDs were prepared by ultrasonication of $MoSe_2$ powders in Pluronic®F127 aqueous solution. As illustrated in

Scheme 1, when water is under intense ultrasonication (tip sonication), acoustic cavitation happens and forms shockwave in localized space, which will cause large $MoSe_2$ flakes collision violently and break up into small pieces, such as nanosheets and nanodots.[34-35] F127 is a non-ionic triblock copolymer (PEO-PPO-PEO) surfactant. During the preparation process, F127 molecules in aqueous solution can absorb onto the surface of $MoSe_2$ NDs, render them water dispersible, and prevent them from aggregation. Moreover, F127 is a biocompatible polymer and have been used for surface functionalization of nanomaterials.[36-37] In order to efficiently separate small $MoSe_2$ NDs from large aggregates, gradient centrifugation was adopted. After ultrasonication, $MoSe_2$ aqueous suspension was first centrifuged at 5000 rpm to sediment the large aggregates. The supernatant was collected and centrifuged at 12000 rpm to separate the $MoSe_2$ nanosheets. Then, ultrasmall $MoSe_2$ NDs can be obtained from the supernatant by further high-speed centrifugation at 21000 rpm.

Characterization of $MoSe_2$ NDs

From the TEM image (Fig. 1a), we can see $MoSe_2$ NDs have uniform dot-like morphology with average size of 2.32±0.69 nm (Fig. S1a, ESI). Clear crystalline structure can be observed from the HRTEM image of $MoSe_2$ NDs (Fig. 1b), and the lattice spacing of 0.21 nm can be ascribed to (104) plane of 2H-$MoSe_2$.[33] Atomic force microscopy (AFM) image (Fig. 1c) shows that the as-prepared $MoSe_2$ NDs have relative heights in the range of 0.7 to 2.1 nm (Fig. 1d), which are similar to the thickness of 1 to 3 layers of 2H-$MoSe_2$.[38] By using dynamic light scattering (DLS), the hydrodynamic size of $MoSe_2$ NDs is determined to be about 7.2 nm (Fig. S1b, ESI), which is larger than the size obtained by TEM and can be ascribed to the adsorption of F127 molecules on the surface of $MoSe_2$ NDs.
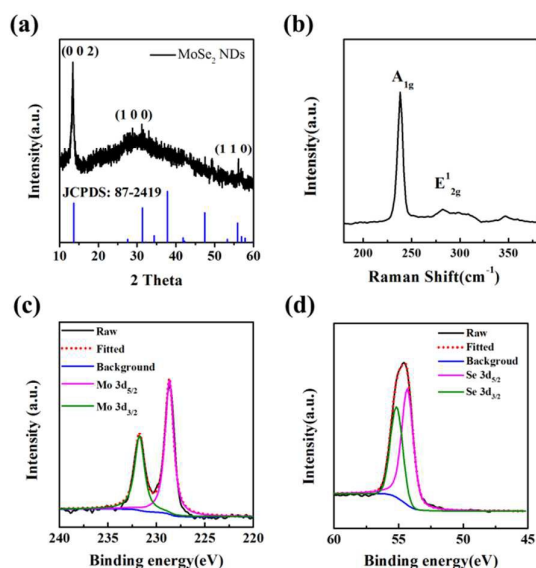
Fig. 2 (a) X-ray diffraction (XRD) pattern of $MoSe_2$ NDs, along with a reference pattern of bulk 2H-$MoSe_2$ (JCPDS: 87-2419); (b) Raman spectrum of $MoSe_2$

NDs; (c) X-ray photoelectron spectroscopy (XPS) spectrum of MoSe₂ NDs for Mo 3d and (d) Se 3d core level energy regions.

Fig. 2a shows the XRD pattern of MoSe₂ NDs. The diffraction peak at 13.4° belongs to the (002) plane, matching the peak position of 2H-MoSe₂ (JCPDS, 87-2419). The distinct (002) peak indicates the existence of few-layers in the c-axis of MoSe₂ NDs. The diffraction peak of (100) plane for MoSe₂ NDs broadens significantly in comparison with bulk MoSe₂, which may originate from the size reduction of MoSe₂ NDs.[39] Raman spectroscopy was used to investigate the structure of MoSe₂ NDs. As depicted in Fig. 2b, two characteristic Raman peaks located at 238.1 cm^{-1} and 282.0 cm^{-1} are associated to the out-of-plane A_{1g} mode and in-plane E^1_{2g} mode, respectively.[40] Compared with bulk MoSe₂ (243 cm^{-1}), the peak position of A_{1g} mode for MoSe₂ NDs exhibits an obvious decrease, which suggests a reduction of the layer thickness.[41] The Raman peak near 346.8 cm^{-1} has been demonstrated to relate with the interlayer interaction and only appears in multi-layered MoSe₂ nanosheets, which hints that MoSe₂ NDs are ultrasmall few-layer nanosheets.[40, 42] XPS was used to study the compositions of the as-prepared MoSe₂ NDs. The region with binding energy from 240 eV to 220 eV can be fitted into doublet peaks located at 231.8 eV and 228.6 eV, which can be attributed to Mo $3d_{3/2}$ and Mo $3d_{5/2}$, respectively, consistent with Mo 4+ oxidation.[39, 43] The absence of the peaks near 236 eV can exclude the formation of Mo oxide in 6+ oxidation state.[41, 44] The 3d core level region of Se can be deconvoluted into doublet peaks located at 55.0 eV and 54.2 eV, which can be ascribed to Se $3d_{3/2}$ and Se $3d_{5/2}$ of Se^{2-}, respectively, suggesting that MoSe₂ NDs haven't been oxidized during the preparation process.[41, 44]

Optical and Photothermal Property
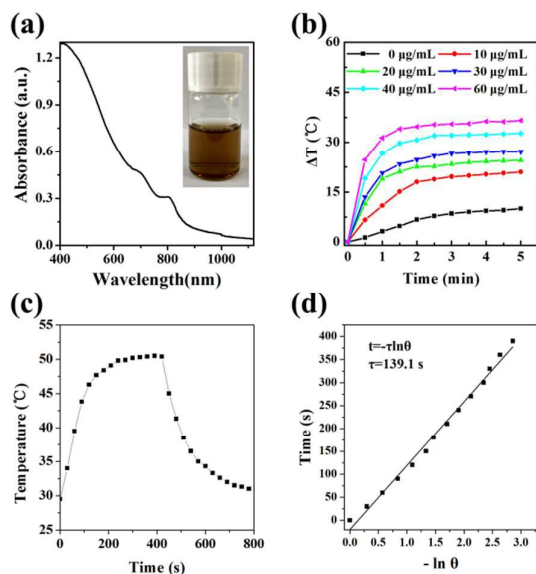
Fig. 3 (a) UV-Vis-NIR spectrum of MoSe₂ NDs suspended in water. Inset: photograph of MoSe₂ NDs aqueous dispersion; (b) Photothermal heating curves of aqueous dispersions of MoSe₂ NDs at different concentrations (10, 20, 30, 40, and 60 μg/mL) under NIR laser irradiation with a power density of 2 W/cm² at 785 nm; (c) Temperature evolution of MoSe₂ NDs aqueous dispersion (10 μg/mL)

during heating (laser on, 400 s) and cooling (laser off, 400 s); (d) Thermal equilibrium time constant of the system determined by fitting the time data versus negative natural logarithm of the driving force temperature from the cooling period.

As we know, MoSe₂ is a selenide of TMDCs with narrow direct band gap (~1.5 eV) and can be used as NIR-responsive optical material;[45-46] while extensively studied transition metal sulphides usually have larger direct band gaps responsive to visible light, such as MoS₂ (~1.8 eV)[47] and WS₂ (~2.0 eV)[48]. Fig. 3a shows the UV-Vis-NIR spectrum of MoSe₂ NDs in aqueous solution. The distinct absorption peak located at about 801 nm (1.55 eV) can be ascribed to the A exciton of 2H-MoSe₂.[45] This NIR absorption peak originates from the transition of the smallest direct band gap at K point of the Brillouin zone.[49] Moreover, no obvious photoluminescence can be detected from the visible to NIR region (500~900 nm) whether using UV or visible light excitation, which is similar to the optical property of few-layer MoSe₂ nanosheets.[40] The coexistence of strong absorption and non-photoluminescence features in MoSe₂ NDs indicate that the excited state of MoSe₂ NDs after light absorption may relax by non-radiative ways to the ground state.

According to Beer-Lambert Law (Eq. 1 and 2, ESI), the mass extinction coefficient (ε) of MoSe₂ NDs at 785 nm can be calculated to be 17.4 $Lg^{-1}cm^{-1}$ (Fig. S3, ESI), which is larger than gold nanorods (13.9 $Lg^{-1}cm^{-1}$, at 808 nm), a commonly used PTT agent.[50] The photothermal property of MoSe₂ NDs was further studied by monitoring the temperature change of MoSe₂ NDs aqueous dispersions under NIR laser irradiation with power density of 2 W/cm² at 785 nm. As shown in Fig. 3b, the temperature change (ΔT) of pure water is only 3 ℃ after 1 min NIR irradiation, while MoSe₂ NDs aqueous dispersions (60 μg/mL) can significantly increase about 31 ℃, revealing the excellent photothermal property of MoSe₂ NDs. In order to compare the light-to-heat conversion capability of MoSe₂ NDs with other PTT agents, the photothermal conversion efficiency (η) is calculated according to the reported methods (the details can be found in ESI).[51] As illustrated in Fig. 3c, by measuring temperature evolution of MoSe₂ NDs aqueous suspensions during heating (laser-on) and cooling (laser-off) processes, thermal equilibrium time constant of the system can be determined to be 139.1 s and the value of η was further determined to be 46.5% (according to Eq. 12 and 14, ESI), which is higher than most of the currently studied PTT agents, such as gold nanoshells (13%), gold nanorods (21%), Cu₂₋ₓSe (22%), and Cu₉S₅ (25.7%).[10, 52] As mentioned above, MoSe₂ NDs have both high extinction coefficient and high photothermal conversion efficiency of NIR light, which are fascinating optical properties but hasn't been fully addressed yet. Compared with the most studied plasmonic PTT agents (gold nanomaterials, copper chalcogenides, etc.), MoSe₂ is a semiconductor material with unique photothermal converting ways. First of all, the absorption peak of MoSe₂ located near 801 nm (A exciton) is direct band gap transition, which is an allowed optical transition and is much stronger than the indirect band gap (1.1 eV) absorption of MoSe₂.[53] The direct band gap of MoSe₂ is located at K point of Brillouin zone, while the

indirect band gap originates from the bottom of the conduction band between Γ and K points, which means that the excited state of A exciton may decay from the K point to the bottom between Γ and K points and greatly enhances the energy transformation from light to heat through exciton-phonon coupling.[54] Hence, we ascribe the excellent photothermal properties of MoSe$_2$ NDs to their unique electronic structure.

Photostability of MoSe$_2$ NDs

The photothermal stability of MoSe$_2$ NDs was also tested. As illustrated in Fig. 4a, before NIR laser irradiation, both MoSe$_2$ NDs and ICG solutions have identical absorbance at 785 nm. After laser irradiation for 30 min (2 W/cm^2 at 785 nm), the absorption peaks of ICG almost completely bleached. In contrast, the absorption spectra of MoSe$_2$ NDs changed little under the same laser irradiation conditions, which obviously proves that MoSe$_2$ NDs have better photostability. During NIR irradiation, the temperature of MoSe$_2$ NDs aqueous dispersion keeps relatively stable, while that of ICG's decreases significantly, which further indicates that MoSe$_2$ NDs is more photostable than the organic PTT agent ICG. Encouraged by their excellent photothermal performance, MoSe$_2$ NDs were further investigated for potential use as PTT agent.
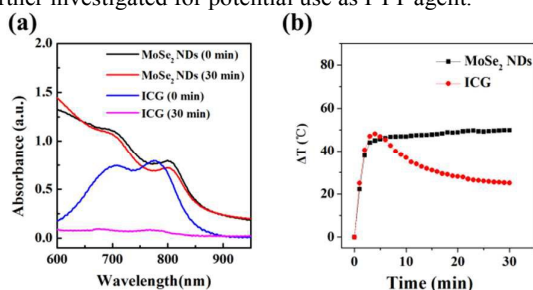
Fig. 4 (a) UV-Vis-NIR absorption spectra of MoSe$_2$ NDs and ICG aqueous dispersions before and after NIR laser irradiation with a power density of 2 W/cm^2 at 785 nm for 30 min; (b) Temperature evolution of MoSe$_2$ NDs and ICG aqueous dispersions during NIR laser irradiation.

Cytotoxicity and Colloidal Stability

Biocompatibility is an important prerequisite for biomedical applications of nanomaterials. Previous studies have shown that transition metal sulphides, such as MoS$_2$ and WS$_2$ nanosheets, have good biocompatibility, but the cytotoxicity of transition metal selenides, especially their nanodot form, haven't been well studied.[55-56] Hence, the cytotoxicity of the MoSe$_2$ NDs was first examined before in vitro experiments. The relative cell viability of HeLa cells incubated with different concentrations of MoSe$_2$ NDs (1.25, 2.5, 5, 10, 20, 40, 80, and 160 μg/mL) was determined by LDH (lactate dehydrogenase) Assay. As demonstrated in Fig. 5a, HeLa cells remain nearly 100% viable after incubated with MoSe$_2$ NDs for 48 h even up to 160 μg/mL, which demonstrates that the as-prepared MoSe$_2$ NDs without further surface modification have good biocompatibility. Moreover, the colloidal stability of MoSe$_2$ NDs has also been tested. As shown in Fig. 5b, after storage at room temperature for 4 days, all three samples of MoSe$_2$ NDs dispersed in water, phosphate buffered saline (PBS), and cell culture medium (DMEM) remain stable and no obvious

aggregation forms. This good colloidal stability of MoSe$_2$ NDs may originate from the PEO block of F127, which can render MoSe$_2$ NDs with hydrophilic surface and low Zeta potential about -17.8 mV, similar to that of pure F127 (Fig. S1c, ESI).

Photothermal Therapy of Cancer Cells

In vitro experiments were further carried out to examine the PTT effect of MoSe$_2$ NDs to cancer cells. As depicted in Fig. 5c, under NIR laser irradiation at 785 nm for 10 min, the relative cell viability of HeLa cells continuously decreases with increasing concentrations of MoSe$_2$ NDs. At a relative low concentration (40 μg/mL), MoSe$_2$ NDs can effectively reduce the viability of HeLa cells to less than 8%. As can be seen from the fluorescence images in Fig. 4d, after NIR photothermal treatment and co-stained with Calcein-AM and PI, the live HeLa cells with green fluorescence gradually decrease, while the dead HeLa cells with red fluorescence obviously increase with the increasing concentrations of MoSe$_2$ NDs and most of the HeLa cells are killed by PTT treatment at the concentration of 40 μg/mL, which suggests that MoSe$_2$ NDs can be potentially used as an efficient PTT agent.
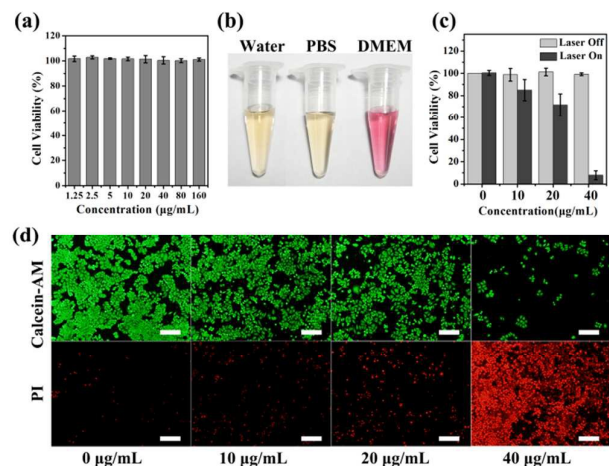
Fig. 5 (a) Cell viability of HeLa cells incubated with different concentrations (1.25, 2.5, 5, 10, 20, 40, 80, and 160 μg/mL) of MoSe$_2$ NDs for 48 h; (b) Photograph of MoSe$_2$ NDs dispersed in water, PBS (20 mM, pH 7.4), and cell culture medium (DMEM) after 4 days storage; (c) Cell viability of HeLa cells with and without 785 nm NIR laser irradiation (2 W/cm^2, 10 min) after incubated with MoSe$_2$ NDs at different concentrations for 12 h; (d) Fluorescence microscopy images of HeLa cells co-stained with Calcein-AM (green fluorescence, live cells) and PI (red fluorescence, dead cells) after incubated with different concentrations (from left to right: 0, 10, 20, and 40 μg/mL) of MoSe$_2$ NDs for 12 h and then irradiated with NIR laser at power density of 2 W/cm^2 at 785 nm for 10 min.

Conclusions

In summary, we have developed a simple and direct aqueous preparation method for ultrasmall MoSe$_2$ NDs by using ultrasonication-assisted liquid exfoliation, which may also be useful to prepare other TMDCs NDs. Due to the unique electronic structure, MoSe$_2$ NDs have both strong absorption in NIR region (17.4 Lg^{-1}cm^{-1} at 785 nm) and excellent photothermal conversion efficiency of 46.5% which is

Nanoscale Accepted Manuscript

significant higher than commonly studied photothermal agents, such as gold nanorods and copper chalcogenides. Moreover, the as-prepared $MoSe_2$ NDs have several other unique features that the ideal photothermal agent needs, such as ultrasmall size (2~3 nm), good colloidal stability, photothermal stability, and biocompatibility. For the first time, $MoSe_2$ NDs has been explored as a novel photothermal agent. Under NIR laser irradiation at 785 nm, $MoSe_2$ NDs can efficiently kill HeLa cells at relatively low concentration (40 μg/mL), which opens up novel opportunities of biomedical applications for TMDCs NDs.

Experimental

Materials

$MoSe_2$ (325 mesh, 99.95%) and Pluronic® F-127 (powder, CMC 950-1000 ppm) were purchased from Sigma-Aldrich. Ultrapure water (Millipore, 18.2 MΩ) was used to prepare all of the aqueous solutions in this study.

Preparation of $MoSe_2$ NDs

In a typical procedure, 3.75 g F-127 powder and 50 mL water were added into a 100 mL glass bottle. The mixture was magnetically stirred until it became clear. Then, 75 mg $MoSe_2$ powder was added into the F127 solution and stirred for 30 min. The aqueous dispersion of $MoSe_2$ powder was sonicated in an ice-bath by using tip sonication (Yimaneili, 950W, 25kHz) with 60% amplitude. The sonication was pulsed for 2s on and 3s off for a total sonication time of 4 h. The aqueous suspension of $MoSe_2$ was centrifuged at 5000 rpm for 30 min to separate the large aggregates. The precipitate was discarded and the supernatant was then centrifuged at 12000 rpm for 30 min. Then, the supernatant was transferred to other centrifuge tubes and centrifuged at 21000 rpm for 30 min. The sediment was collected and redispersed in water. Further centrifugation at 21000 rpm for 30 min was repeated at least two times. At last, the precipitate was dispersed in ultrapure water and stored at 4 ℃.

Cell Culture

The HeLa cells (human cervical cell line, KeyGEN BioTECH) were cultured in DMEM medium (KeyGEN BioTECH) supplemented with 10% fetal bovine serum (FBS, Gibco), 80 U/mL penicillin, and 0.08 mg/mL streptomycin at 37℃ under 5% CO_2. The cells were detached by Trypsin-EDTA solution (0.25 w/v % trypsin and 0.02 w/v % EDTA), and were then rinsed, centrifuged, and resuspended in DMEM medium.

In vitro Cytotoxicity Assay

The relative cell viability was evaluated with LDH-Cytotoxicity Colorimetric Assay Kit (BioVision). The cells ($1*10^4$) were seeded on 96 multi-well plates, and incubated overnight. The culture medium was removed and 150 μL of DMEM (no FBS) with varying concentrations of $MoSe_2$ NDs (1.25, 2.5, 5, 10, 20, 40, 80, and 160 μg/mL) were added into 4 wells, respectively. Cells cultured with DMEM medium were used as Background Control, cells cultured without any $MoSe_2$ NDs as Low Control, and cells with medium containing 1% Triton X-100 as High Control. After being incubated for 48 h, 100 μL supernatant of each well was transferred carefully into corresponding wells of optically clear 96 multi-well plates. After adding 100 μL reaction mixtures (containing 0.25 mL catalyst solution and 11.25 mL dye solution) to each well, the plates were incubated for 15 min at room temperature, and protected from light. The absorbance of all samples at 495 nm was measured by a microtiter plate reader (PowerWave XS2, BioTek). The viability of cells was calculated using the formula as follows:

Cell viability = 100% - (Test Sample - Low Control) / (High Control - Low Control)*100%

In vitro Photothermal Therapy

HeLa cells ($1*10^4$) were seeded in 96-well plates and incubated with $MoSe_2$ NDs suspensions of different concentrations (0, 10, 20, and 40 μg/mL) in DMEM medium for 12 h. After being washed with PBS, 50 μL DMEM medium was added and cells were irradiated by a 785 nm NIR laser at power density of 2 W/cm^2 for 10 min. More DMEM medium (100 μL) was added into each well. After incubated for 12 h, 100 μL supernatant from each well was transferred and the relative cell viability was measured with LDH-Cytotoxicity Colorimetric Assay Kit as described before. The remained HeLa cells in 96-well plates were co-stained with Calcein-AM and PI (KeyGEN BioTECH) for 30 min, washed with PBS, and imaged by motorized inverted fluorescence microscope (Olympus IX71, Japan).

Acknowledgements

Notes and references

†Electronic Supplementary Information (ESI) available: Characterization, Size distribution and EDS spectrum of $MoSe_2$ NDs, Calculation of extinction coefficient and photothermal conversion efficiency of $MoSe_2$ NDs.

[1] C. P. Nolsøe, S. Torp-Pedersen, F. Burcharth, T. Horn, S. Pedersen, N. E. Christensen, E. S. Olldag, P. H. Andersen, S. Karstrup, T. Lorentzen, *Radiology* 1993**,** 187, 333.

[2] K. McMillan, I. Perepelitsyn, Z. Wang, S. M. Shapshay, *Cancer Lett.* 1999**,** 137, 35.

[3] L. Cheng, C. Wang, L. Feng, K. Yang, Z. Liu, *Chem. Rev.* 2014**,** 114, 10869.

[4] D. Jaque, L. Martinez Maestro, B. del Rosal, P. Haro-Gonzalez, A. Benayas, J. L. Plaza, E. Martin Rodriguez, J. Garcia Sole, *Nanoscale* 2014**,** 6, 9494.

[5] S. Lal, S. E. Clare, N. J. Halas, *Acc. Chem. Res.* 2008**,** 41, 1842.

[6] H. Tang, C. M. Hessel, J. Wang, N. Yang, R. Yu, H. Zhao, D. Wang, *Chem. Soc. Rev.* 2014, 43, 4281.

[7] J. Qi, X. Lai, J. Wang, H. Tang, H. Ren, Y. Yang, Q. Jin, L. Zhang, R. Yu, G. Ma, Z. Su, H. Zhao, D. Wang, *Chem. Soc. Rev.* 2015**,** 44, 6749.

[8] N. W. S. Kam, M. O'Connell, J. A. Wisdom, H. Dai, *Proc. Nat. Acad. Sci. U.S.A.* 2005, 102, 11600.

[9] K. Yang, S. Zhang, G. Zhang, X. Sun, S.-T. Lee, Z. Liu, *Nano. Lett.* 2010, 10, 3318.

[10] Q. Tian, F. Jiang, R. Zou, Q. Liu, Z. Chen, M. Zhu, S. Yang, J. Wang, J. Wang, J. Hu, *ACS Nano* 2011**,** 5, 9761.

[11] I. H. El-Sayed, X. Huang, M. A. El-Sayed, *Cancer Lett.* 2006, 239, 129.

[12] L. R. Hirsch, R. J. Stafford, J. A. Bankson, S. R. Sershen, B. Rivera, R. E. Price, J. D. Hazle, N. J. Halas, J. L. West, *Proc. Nat. Acad. Sci. U.S.A.* 2003**,** 100, 13549.

[13] X. Huang, I. H. El-Sayed, W. Qian, M. A. El-Sayed, *J. Am. Chem. Soc.* 2006, 128, 2115.

[14] J. Yang, J. Choi, D. Bang, E. Kim, E.-K. Lim, H. Park, J.-S. Suh, K. Lee, K.-H. Yoo, E.-K. Kim, Y.-M. Huh, S. Haam, *Angew. Chem. Int. Ed.* 2011**,** 50, 441.

[15] X. Song, Q. Chen, Z. Liu, *Nano Res.* 2014**,** 8, 340.

[16] W. R. Chen, R. L. Adams, A. K. Higgins, K. E. Bartels, R. E. Nordquist, *Cancer Lett.* 1996**,** 98, 169.

[17] W. Holzer, M. Mauerer, A. Penzkofer, R. M. Szeimies, C. Abels, M. Landthaler, W. Bäumler, *J. Photochem. Photobiol., B* 1998**,** 47, 155.

[18] M. Longmire, P. L. Choyke, H. Kobayashi, *Nanomedicine* 2008**,** 3, 703.

[19] M. Zhou, J. Li, S. Liang, A. K. Sood, D. Liang, C. Li, *ACS Nano* 2015**,** 9, 7085.

[20] Z. Sun, H. Xie, S. Tang, X. F. Yu, Z. Guo, J. Shao, H. Zhang, H. Huang, H. Wang, P. K. Chu, *Angew. Chem. Int. Ed.* 2015**,** 54, 11526.

[21] J. Mou, P. Li, C. Liu, H. Xu, L. Song, J. Wang, K. Zhang, Y. Chen, J. Shi, H. Chen, *Small* 2015**,** 11, 2275.

[22] S. Tang, M. Chen, N. Zheng, *Small* 2014**,** 10, 3139.

[23] M. Chhowalla, H. S. Shin, G. Eda, L.-J. Li, K. P. Loh, H. Zhang, *Nat. Chem.* 2013**,** 5, 263.

[24] X. Huang, Z. Zeng, H. Zhang, *Chem. Soc. Rev.* 2013**,** 42, 1934.

[25] D. Gopalakrishnan, D. Damien, M. M. Shaijumon, *ACS Nano* 2014**,** 8, 5297.

[26] S. Xu, D. Li, P. Wu, *Adv. Funct. Mater.* 2015**,** 25, 1127.

[27] C. Zhu, X. Mu, P. A. van Aken, Y. Yu, J. Maier, *Angew. Chem. Int. Ed.* 2014**,** 53, 2152.

[28] H. D. Ha, D. J. Han, J. S. Choi, M. Park, T. S. Seo, *Small* 2014**,** 10, 3858.

[29] L. Lin, Y. Xu, S. Zhang, I. M. Ross, A. C. Ong, D. A. Allwood, *ACS Nano* 2013**,** 7, 8214.

[30] D. Gopalakrishnan, D. Damien, B. Li, H. Gullappalli, V. K. Pillai, P. M. Ajayan, M. M. Shaijumon, *Chem. Commun.* 2015**,** 51, 6293.

[31] Y. Wang, Y. Ni, *Anal. Chem.* 2014**,** 86, 7463.

[32] L. Jiang, H. Zeng, *Nanoscale* 2015**,** 7, 4580.

[33] X. Zhang, Z. Lai, Z. Liu, C. Tan, Y. Huang, B. Li, M. Zhao, L. Xie, W. Huang, H. Zhang, *Angew. Chem. Int. Ed.* 2015**,** 54, 5425.

[34] K. S. Suslick, *Science* 1990**,** 247, 1439.

[35] V. Nicolosi, M. Chhowalla, M. G. Kanatzidis, M. S. Strano, J. N. Coleman, *Science* 2013**,** 340, 1420.

[36] S. H. Lee, J. E. Lee, W. Y. Baek, J. O. Lim, *J. Control. Release* 2004**,** 96, 1.

[37] B. D. Holt, P. A. Short, A. D. Rape, Y.-l. Wang, M. F. Islam, K. N. Dahl, *ACS Nano* 2010**,** 4, 4872.

[38] Y. H. Chang, W. Zhang, Y. Zhu, Y. Han, J. Pu, J. K. Chang, W. T. Hsu, J. K. Huang, C. L. Hsu, M. H. Chiu, T. Takenobu, H. Li, C. I. Wu, W. H. Chang, A. T. Wee, L. J. Li, *ACS Nano* 2014**,** 8, 8582.

[39] D. Sun, S. Feng, M. Terrones, R. E. Schaak, *Chem. Mater.* 2015**,** 27, 3167.

[40] P. Tonndorf, R. Schmidt, P. Böttger, X. Zhang, J. Börner, A. Liebig, M. Albrecht, C. Kloc, O. Gordan, D. R. T. Zahn, S. Michaelis de Vasconcellos, R. Bratschitsch, *Opt. Express* 2013**,** 21, 4908.

[41] G. W. Shim, K. Yoo, S. B. Seo, J. Shin, D. Y. Jung, I. S. Kang, C. W. Ahn, B. J. Cho, S. Y. Choi, *ACS Nano* 2014**,** 8, 6655.

[42] D. Kong, H. Wang, J. J. Cha, M. Pasta, K. J. Koski, J. Yao, Y. Cui, *Nano. Lett.* 2013**,** 13, 1341.

[43] W. e. A. Abdallah, A. E. Nelson, *J. Mater. Sci.* 2005**,** 40, 2679.

[44] X. Wang, Y. Gong, G. Shi, W. L. Chow, K. Keyshar, G. Ye, R. Vajtai, J. Lou, Z. Liu, E. Ringe, B. K. Tay, P. M. Ajayan, *ACS Nano* 2014**,** 8, 5125.

[45] A. M. Goldberg, A. R. Beal, F. A. Lévy, E. A. Davis, *Philos. Mag.* 1975**,** 32, 367.

[46] A. Anedda, E. Fortin, *J. Phys. Chem. Solids* 1980**,** 41, 865.

[47] C. B. Roxlo, R. R. Chianelli, H. W. Deckman, A. F. Ruppert, P. P. Wong, *J. Vac. Sci. Technol., A* 1987**,** 5, 555.

[48] A. R. Beal, W. Y. Liang, *J. Phys. C: Solid State Phys.* 1976**,** 9, 2459.

[49] R. Coehoorn, C. Haas, R. A. de Groot, *Phys. Rev. B* 1987**,** 35, 6203.

[50] J. Robinson, K. Welsher, S. Tabakman, S. Sherlock, H. Wang, R. Luong, H. Dai, *Nano Res.* 2010**,** 3, 779.

[51] D. K. Roper, W. Ahn, M. Hoepfner, *J. Phys. Chem. C* 2007**,** 111, 3636.

[52] C. M. Hessel, V. P. Pattani, M. Rasch, M. G. Panthani, B. Koo, J. W. Tunnell, B. A. Korgel, *Nano. Lett.* 2011**,** 11, 2560.

[53] K. K. Kam, B. A. Parkinson, *J. Phys. Chem.* 1982**,** 86, 463.

[54] S. Tongay, J. Zhou, C. Ataca, K. Lo, T. S. Matthews, J. Li, J. C. Grossman, J. Wu, *Nano. Lett.* 2012**,** 12, 5576.

[55] W. Yin, L. Yan, J. Yu, G. Tian, L. Zhou, X. Zheng, X. Zhang, Y. Yong, J. Li, Z. Gu, Y. Zhao, *ACS Nano* 2014**,** 8, 6922.

[56] L. Cheng, J. Liu, X. Gu, H. Gong, X. Shi, T. Liu, C. Wang, X. Wang, G. Liu, H. Xing, W. Bu, B. Sun, Z. Liu, *Adv. Mater.* 2014**,** 26, 1886.